Adipocyte Na, K-ATPase signaling attenuates experimental uremic cardiomyopathy

Komal Sodhi[*], Xiaoliang Wang, Muhammad A. Chaudhary, Hari Vishal Lakhani, Mishghan Zehra, Athar Nawab, Cameron L. Cottrill, Fang Bai, Jiang Liu, Juan R. Sanabria, Zijian Xie[$], Joseph I. Shapiro

Departments of Medicine, Surgery, and Biomedical Sciences, Joan C. Edwards School of Medicine, Marshall University, Huntington, WV, USA

$In memory of a scientist, and mentor.

ABSTRACT

Oxidative stress has been shown to cause an alteration of intracellular signaling in adipocytes that may lead to various comorbidities of obesity and cardiovascular complications. Evidence suggests that dysregulation of Na, K-ATPase signaling can contribute to systemic inflammation and redox signaling that leads to various metabolic disturbances. Hence the present study aims to explore the specific role of adipocyte Na, K-ATPase signaling in the amelioration of pathophysiological alterations of experimental uremic cardiomyopathy. Experimental uremic cardiomyopathy was induced by partial nephrectomy (PNx), and adipocyte-specific expression of NaKtide, a peptide that inhibits Na, K-ATPase signaling, was achieved using a lentivirus construct with NaKtide expression driven by an adiponectin promoter. Cardiomyopathy and anemia induced in partial nephrectomy mice were accompanied by an altered molecular phenotype of adipocytes, increased systemic inflammatory cytokines and oxidant stress within 4 weeks. These changes were significantly worsened by the addition of a Western diet (enriched in fat and fructose contents) but were prevented with specific expression of NaKtide in adipocytes. The skeletal muscle-specific expression of NaKtide did not ameliorate the disease phenotype. Adipocyte dysfunction and uremic cardiomyopathy developed in PNx mice, both were significantly ameliorated by the adipocyte-specific expression of NaKtide. These findings suggest that oxidative milieu in the adipocyte has a pivotal role in the development and progression of uremic cardiomyopathy in mice subjected to partial nephrectomy. If confirmed in humans, this may be a lead for future research to explore novel therapeutic targets in chronic renal failure.

Introduction

Evidence suggests that adipocyte dysfunction has been instrumental in the pathogenesis of obesity-associated systemic oxidant stress and the comorbidities of obesity including insulin resistance, accelerated cardiovascular disease and non-alcoholic steatohepatitis (1-3). Studies demonstrate that systemic oxidative stress during obesity can be initiated and sustained over time by dysfunctional adipocytes that secrete inflammatory adipokines and reactive oxygen species (ROS) (4-7). Hence, this dysregulated adipokine secretion and inflammation might be a cause and consequence of the activation of oxidative stress signaling pathways in adipose tissue and thereby acts as a potential contributor to the higher susceptibility for metabolic diseases (4). Obesity-related chronic metabolic dysregulations such as hyperglycemia, insulin resistance, and hyperlipidemia along with deranged mitochondrial function, further exacerbate the systemic oxidative stress and chronic inflammation (8-10). As the aforementioned metabolic irregularities are all implicated in the pathogenesis of uremic cardiomyopathy, we aimed to explore the pivotal role of adipocytes in the progression of this condition.

Chronic Kidney disease (CKD) is prevalent in the United States and the common complication of CKD is cardiovascular disease, which affects almost 69.6% of the afflicted population (11). Uremic Cardiomyopathy is an irreversible cardiovascular complication in which oxidant stress plays a key role in the disease progression (12, 13). The prevalence of cardiovascular complications parallels the decline in renal function. Cardiac dysfunction mediated by myocardial fibrosis and asymmetric ventricular hypertrophy are the main features of uremic cardiomyopathy (14). Previous studies suggest that uremic toxins accumulate in the sera of CKD patients, resulting in both oxidative stress and the production of proinflammatory cytokines that contribute to the pathophysiology (15). Oxidant stress and the production of ROS are subsequently exacerbated by the excessive release of cytokines, including IL-6, TNF-α, and MCP-1, whose systemic concentrations correlate positively with the advancing stage of CKD (10).

The sodium-potassium adenosine triphosphatase (Na, K-ATPase), a P-type ATPase, has a signaling function that augments oxidative stress in addition to its pumping function (16-18). In addition to ouabain or other cardiotonic steroids, ROS also acts as activators of Na, K-ATPase signaling (18-22). ROS-mediated carbonylation of the α1 subunit of Na, K-ATPase activates c-Src signaling cascade with downstream activation of extracellular signal-regulated kinase 1/2 (ERK1/2), which in turn creates

a feed-forward oxidant amplification loop (NKAL) that further accelerates cellular oxidative stress.(23-25). Thus a 20-amino acid sequence peptide, NaKtide, has been discovered from the ND1 segment of α1 to inhibit Na, K-ATPase signaling and prevent the activation of c-Src (26). pNaKtide, the cell-permeable version of NaKtide, has been reported to ameliorate functional and metabolic manifestations of obesity and comorbidities characterized by systemic oxidant stress (26-30) We have already shown that systemic administration of pNaKtide attenuates uremic cardiomyopathy, which led to the basis for our current hypothesis (27). Hence, the present study investigates the specific role of adipocyte NKAL in the pathogenesis of experimental uremic cardiomyopathy.

Lentiviral vectors are incredibly effective genetic manipulators in the field of gene and cell therapy due to their remarkable ability to integrate transgenes into the host cell genome efficiently (31). They have been used as a convenient and safe tool for stable gene transfer, using a promoter for a specific cell type, in different experimental models (32-36). We, therefore, chose this strategy to test the hypothesis that adipocyte oxidant stress plays a central role in the pathogenesis of uremic cardiomyopathy.

Materials and Methods

Experimental design for in vivo studies

Male C57Bl6 mice (10-12 weeks old) were purchased from Hilltop Laboratory and all animal studies were approved by the Marshall University Animal Care Committee in accordance with the National Institutes of Health (NIH) Guidelines for Care and Use of Laboratory Animals. Mice were housed in a pathogen-free animal research facility in designated rooms equipped with cages that supplied purified air under a 12-h light/dark cycle. Mice were fed a normal chow diet with *ad libitum* access to water or were fed a western diet (WD) with *ad libitum* access to the high-fructose solution. WD-containing fructose has already been established as a model of diet-induced oxidative stress . The composition of WD (Envigo) was 42% fat, 42.7% carbohydrate, and 15.2% protein, yielding 4.5 KJ/g of energy. Fructose water was given at a concentration of 42 g/L, yielding 0.168 KJ/mL of energy. 5/6-nephrectomy (PNx) surgeries were performed on these mice to mimic uremic cardiomyopathy, as described previously and WD was started in the appropriate experimental groups on the day of surgery (27). A two-step surgical approach was employed in the PNx model. At first, the superior and inferior poles of the left kidney were surgically ligated so only one-third of the left kidney mass is functional. The right kidney was removed in the second stage of surgery 7 days post-ligation. The two-step surgical procedure was repeated in sham controls, without the ligation of the left kidney and removal of the right kidney. A milder model of chronic renal failure, 4/6-nephrectomy, was also used to explore the role of renal dysfunction in the pathophysiology of uremic cardiomyopathy. Briefly, in 4/6-nephrectomy, the superior pole of the left kidney was ligated followed by the second surgery to remove the right kidney 7 days later. The cardiac phenotype of sham mice fed with WD didn't show any significant alterations compared to sham mice fed with normal chow. Echocardiographic measurements were used to evaluate the cardiac phenotype, including LVM (Sham: 90.1mg ± 2.3; Sham+WD: 91.7mg ± 2.5)

and MPI (Sham: 0.42 ± 0.02; Sham+WD: 0.43 ± 0.01).

To yield the adipocyte-specific expression, lentiviral vectors expressing either GFP-NaKtide or GFP cDNA under the control of an adiponectin promoter were constructed (VectorBuilder Inc). Lentiviral constructs featured the adiponectin promoter driving expression of the NaKtide cassette linked by means of a 2A peptide to GFP for bicistronic expression. The 2A peptides are a class of 18-22 amino acid-long self-cleaving peptide that maintains each protein as its own domain. Among the 2A peptides family, T2A was used for our lentiviral construct. Lentivirus (100 μL, $2×10^9$ TU/mL) with NaKtide or its counterpart Lenti-GFP in saline was intraperitoneally (IP) -injected into C57Bl6 mice, on the same day of PNx surgery. An adipocyte-specific lentiviral vector expressing scrambled NaKtide (adipo-sNaKtide) was used as a control for NaKtide expression. It has been previously established that the expression of sNaKtide, a 20-amino acid mutant peptide (MTVAHMWFDNQIHEADTTEN), does not alter Src kinase activity (26).

Similar to the adipocyte-specific NaKtide, a skeletal muscle-specific NaKtide (myoD-NaKtide) was constructed (VectorBuilder Inc) and preliminary studies were performed in PNx using IP and intravenous (IV) administration to select the most effective route of administration in skeletal muscle. No significant difference in the expression of NaKtide was observed in the immunofluorescence analysis of myoD-NaKtide-treated mice administrated via IP and IV routes (data not shown). Furthermore, no significant changes were observed in either heart weight (IP: 0.172mg ± 0.004; IV: 0.168mg ± 0.004) or hematocrit levels (IP: 37.53 ± 0.96; IV: 36.80 ± 1.53). Hence, because of the ease of administration, we employed IP injections for myoD treatments for subsequent studies.

Mice were randomly divided into five primary groups as follows: (1) Sham, (2) PNx, (3) PNx+adipo-NaKtide, (4) PNx+WD and (5) PNx+WD+adipo-NaKtide. Body weights of mice were measured every week during the course of the experiment and mice in each group were sacrificed after 4 weeks of PNx with or without adipo-NaKtide and dietary interventions. At the time of sacrifice, weights of total body, visceral fat, and heart were determined. A cardiac puncture was performed to collect blood samples, followed by plasma separation and storage at -80°C for measurement of plasma biomarkers. Hematocrit (HCT) was measured with an HCT centrifuge as per the manufacturer's instructions. Tissues were flash-frozen in liquid nitrogen and maintained at -80°C, preserved in OCT for sectioning, or placed in paraformaldehyde for paraffin embedding.

Thiobarbituric acid reactive substances (TBARS) measurement in adipose tissue

TBARS assay kit (Cayman Chemical, Ann Arbor, MI) was used to measure oxidative stress in adipose tissue as per the manufacturer's protocol. Data were presented as μmoles per milligram of protein after normalizing with the total protein content.

Measurement of plasma creatinine and cystatin C

Mouse creatinine assay kit (Crystal Chem Inc., Downers Grover, IL) and Mouse cystatin C ELISA kit (Downers Grove, IL) were used to measure plasma creatinine and cystatin C respectively, according to the manu-

facturer's protocol.

Glucose tolerance test (GTT)

GTT was performed at the end of the 4-week period. After 8 hours of the fasting period, mice were injected (IP) with 10% glucose solution (2g/kg body weight). Blood samples were collected from the tail vein at 0, 30, 60, 90, and 120 minutes after glucose injection and blood glucose was measured using a glucometer.

Histological examination of cardiac tissue

After fixing in 4% paraformaldehyde for 24h at 4°C, the cardiac tissues were washed with PBS, dehydrated and kept in 70% ethanol. After paraffin embedding, microtome sections were cut (5 μm) and stained in picro-sirius red (Solution A) and in fast green solution (Solution B) as previously described (37). The slides were mounted with mounting medium after washing and covered with coverslips. Images were captured in phase contrast microscopy and quantified using ImageJ software.

Measurement of c-Src phosphorylation

The visceral adipose tissue homogenates were prepared with RIPA buffer and phosphorylation of c-Src was determined as described previously (27). After immunoblotting for phospho-Src using polyclonal anti-Src [pY418] phospho-specific antibody (Invitrogen, Camarillo, CA), the same membrane was stripped and blotted for total c-Src using a monoclonal total c-Src antibody (Santa Cruz, CA). Activation of c-Src was expressed as the ratio of phospho-Src/c-Src with measurements normalized to control samples.

Measurement of plasma leptin, cytokines, and protein carbonylation

Plasma levels of inflammatory cytokines such as tumor necrosis factor-alpha (TNFα), interleukin 6 (IL-6), monocyte chemoattractant protein-1 (MCP-1) and leptin were measured using an ELISA kit according to manufacturer instructions (Abcam Cambridge, MA). Protein Carbonyl ELISA Kit (BioCell Corporation, New Zealand) was used to measure the level of protein carbonylation in adipose and heart tissues.

Measurement of tissue-specific NaKtide concentration by competitive ELISA

The concentration of NaKtide was determined using competitive ELISA. Briefly, polystyrene 96-well microtiter plates were coated with 100 μL/well of NaKtide antigen in 1% Dimethyl sulfoxide (DMSO) at a concentration of 50 ng/ml and the plates were incubated overnight at 4°C. After washing the plates thrice with wash buffer (1X PBS and 0.05% Tween-20), blocking was done using 200 μL/well of blocking buffer (1X PBS and 3% BSA) at 37°C for 2 h. Serial dilutions of NaKtide standards (0, 0.025μg/mL, 0.050μg/mL, 0.125μg/mL, 0.25μg/mL, 0.50μg/mL and 1.0μg/mL) were prepared in 1% DMSO. After homogenizing the adipose and skeletal muscle tissues in RIPA Buffer, the protein quantification was performed to normalize the final concentration to 1mg/mL. Thereafter, we performed the deproteinization with Perchloric acid (PCA), followed by neutralization with 1 N NaOH and extraction with chloroform. A mixture of 60uL of NaKtide standards or samples and 60uL of primary NaKtide antibody (1:1000

dilution in 1X PBS and 1% BSA Buffer solution) were prepared and incubated for 1 h at 37°C with gentle shaking. After washing the plates thrice, 100 μL of the sample/antibody or standard/antibody mixtures were pipetted into the wells and the plates were incubated at 37°C for 1 h. The wash step was repeated and 100uL solution of goat anti-rabbit IgG HRP conjugated secondary antibody (1:2000 in dilution buffer) was added in each well and incubated for an additional 1 h at 37°C. 100uL/well of the TMB substrate solution was added into the wells after the washing steps and incubated for the plates for 20 min in the dark, followed by the addition of 50uL stop solution (1M HCl solution). The optical density of each well was read at 450nm wavelength and the concentrations of NaKtide in the samples were calculated based on the standard curve.

The absorbance (O.D. value) of the standard (x-axis) was plotted against the concentration of the standard (y-axis) to generate a standard curve as an XY scatter plot to get a 7-point curve. A polynomial order 3 trendlines was added to the graph to get the line of best fit. The line of best fit for the standard curve was ensured to have a coefficient of determination (R^2 value) of ≥0.98. The unknown concentration of NaKtide in each sample was calculated based on the equation of the line of best fit.

RNA extraction and real time PCR

Total RNA, extracted from adipose and cardiac tissue using RNeasy Protect Mini Kit (QIAGEN, Maryland), was analyzed by a quantitative real-time PCR. Real-time PCR reaction was performed in triplicate using SYBR Green PCR Master Mix on a 7500 HT Fast Real-Time PCR System and the experimental samples were normalized using the housekeeping gene, GAPDH. Specific predesigned primers (IDT DNA Technologies) used for PCR include, TNFα, IL-6, Leptin, toll like receptor 4 (TLR4), TNF receptor-associated factor 6 (TRAF6), peroxisome proliferator-activated receptor g coactivator-1a (PGC-1α), sirtuin 3 (Sirt3), Caspase 9 (Casp9), Collagen 1 (Col1), Bcl2-associated X (Bax), F4/80, and friend leukemia integration 1 (Fli-1).

Immunofluorescence studies in adipose, heart, aorta, and skeletal muscle tissues

Immunofluorescence studies were performed on cryosections (6μm) of frozen tissues in OCT compound. The sections, mounted onto slides, were fixed with 4% PFA for 15 minutes, washed once with TBS-T (1x TBS and 0.025% Triton X-100), blocked in 3% BSA in TBS (2 hours) and probed with 1:30 primary antibody in 1X TBS with 1% BSA overnight at 4°C. After washing with TBS-T twice, 1:1000 secondary antibody (Alexa Fluor 647 Red) was added, incubated for 1 hour at RT, and then mounted with DAPI solution. Expression of lenti-adipo-GFP and lenti-adipo-NaKtide was determined, using a green fluorescent protein (GFP) and Red fluorescent protein (RFP) filter respectively, on a Nikon Eclipse 80i microscope equipped with a Nikon camera head DS-Fi1 (Nikon, Japan).

In order to calculate the percentage of transduction of the lentivirus, number of DAPI and adipocytes was determined using a modified adipocyte count protocol and ImageJ software (NIH) (38). In brief, fluorescent images were opened in ImageJ, changed to 8-bit, converted to mask using the binary function, and enhanced. To ensure an accurate representation of nuclei and adipocytes, black

and white images were compared to the original image. The total number of nuclei and adipocytes was determined, using the "analyze particles" command; the size of the sample was normalized based on the number of pixels present in the image and the magnification. The percentage of transduction efficiency was represented as the ratio of adipocytes to nuclei.

Transthoracic echocardiography

Transthoracic echocardiography (TTE) was performed 24 hours prior to the sacrifice. As described previously (27), B-mode was used for measuring left-ventricular end-diastolic area (EDA), end-systolic area (ESA), and main pulmonary artery diameter. End-diastolic diameters (EDDs), end-systolic diameters (ESDs), and anterior and posterior wall thickness (AWT & PWT) were captured using the M-mode. Isovolumic contraction and relaxation time (IVCT & IVRT), ejection time (ET), as well as pulmonary velocity time integral (VTI), were obtained from PW and color Doppler. The following cardiac characteristics were calculated from the data: myocardial performance index=(IVCT+IVRT)/ET, relative wall thickness (RWT)=(PWT+AWT)/EDD, cardiac output (CO)=stroke volume×HR/1000, fractional shortening=(EDD − ESD)/EDD, ejection fraction (EF)=(EDV − ESV)/EDV and the left ventricular mass index (LVMI)=1.05[(EDD+PWT+AWT)3 − EDD3]/ body weight (g).

Statistical analyses

Results are analyzed and presented as box-and-whisker plots. Data are presented as the median (central line), upper and lower quartiles and whiskers (extreme values) from independent experiments. To identify the statistical significance, groups were compared by analysis of variance (ANOVA), followed by Tukey's post hoc test using GraphPad Prism version 9 (GraphPad, San Diego, CA, USA). Statistical significance was assigned at $p<0.05$ or $p<0.01$ for a confidence interval of 95% or 99%, respectively.

Results

Efficacy and specificity of adipocyte-specific lentiviral transduction of NaKtide in adipose tissue of PNx mice

Immunofluorescence staining was performed to test the effective lentiviral transduction of adiponectin-GFP-NaKtide (adipo-NaKtide) construct in adipose tissues. Visceral adipose tissues of adipo-NaKtide transduced PNx mice showed readily detectable green fluorescence (GFP) and red fluorescence (NaKtide), confirming adipocyte-specific presence of NaKtide (Fig. 1A). Furthermore, using the merged immunofluorescent DAPI, GFP and RFP images, we determined the number of cells transduced by the adipocyte-specific lentiviral construct, which showed a significantly higher percentage of NaKtide transduction in the visceral adipose tissue of PNx mice (Fig. 1B). Subsequently, immunofluorescence staining in subcutaneous adipose tissues of adipo-NaKtide transduced PNx mice showed similar expression of green fluorescence (GFP) and red fluorescence (NaKtide) expression (Fig. S1A). The subcutaneous adipose tissues also showed a significantly high percentage of NaKtide transduction by the adipocyte-specific lentiviral construct, similar to the transduction efficiency observed in visceral adipose tissues (Fig. S1B). The

presence of NaKtide in visceral and subcutaneous adipose tissues was further confirmed by determining the concentration of NaKtide, using competitive ELISA, that we developed. Notably, our analysis showed significant NaKtide concentration in adipo-NaKtide transduced Sham and PNx mice, which was at comparable levels, while levels of NaKtide were undetectable in mice transduced with adipo-GFP (Fig. 1C and S1C). Furthermore, our results confirmed there were no off-target effects of adipo-NaKtide as immunofluorescence staining of skeletal muscle, heart and aorta did not show detectable expression of green fluorescence (GFP) and red fluorescence (NaKtide), further demonstrating the specificity of adipo-NaKtide lentiviral transduction to adipocytes (Fig. S2).

Adipo-NaKtide attenuates oxidative stress and inhibits downstream signaling through antagonism of Na, K-ATPase signaling in adipose tissue of PNx mice

Transduction of adipo-NaKtide resulted in marked reduction of oxidative stress in the adipose tissues of PNx and PNx+WD mice, as determined by TBARS assay (Fig. 1D). Our results further showed that mice fed WD, following PNx surgery, had greater extent of oxidative stress in adipose tissues, as assessed by levels of protein carbonylation, as compared to PNx mice alone (Fig. 1E). Adipo-NaKtide transduction significantly ameliorated protein carbonylation in PNx and PNx+WD mice (Fig. 1E). We have previously shown that carbonylation of the Na/K-ATPase α1 subunit, phosphorylates Src and initiates a downstream signaling cascade (27). Thus, we evaluated the levels of phosphorylated cellular Src (p-Src) in the adipose tissues of PNx mice, with and without WD. PNx
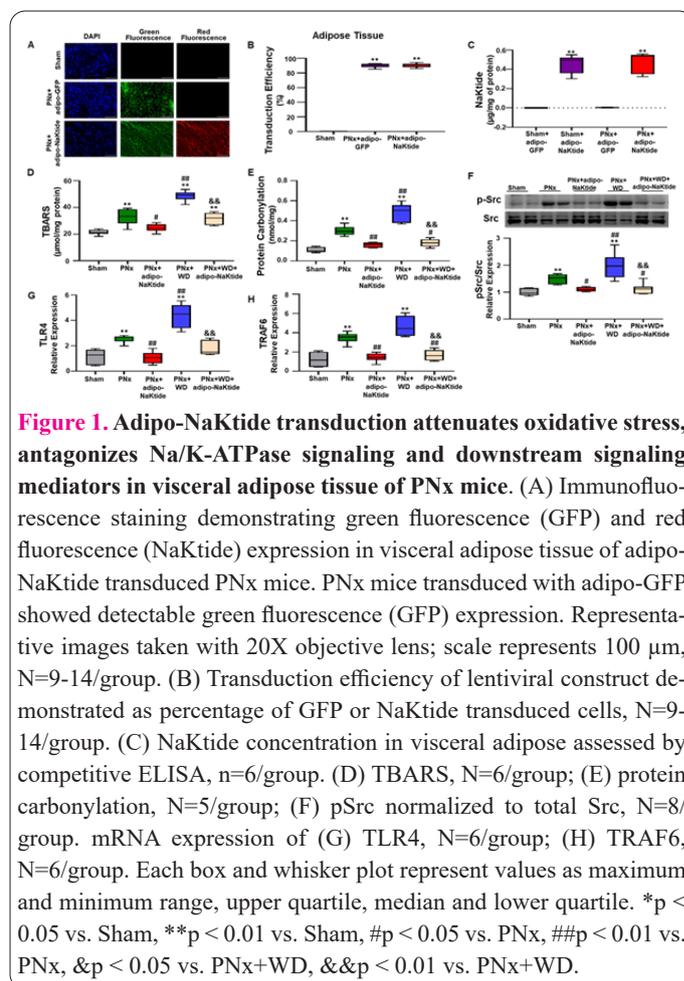
Figure 1. **Adipo-NaKtide transduction attenuates oxidative stress, antagonizes Na/K-ATPase signaling and downstream signaling mediators in visceral adipose tissue of PNx mice**. (A) Immunofluorescence staining demonstrating green fluorescence (GFP) and red fluorescence (NaKtide) expression in visceral adipose tissue of adipo-NaKtide transduced PNx mice. PNx mice transduced with adipo-GFP showed detectable green fluorescence (GFP) expression. Representative images taken with 20X objective lens; scale represents 100 μm, N=9-14/group. (B) Transduction efficiency of lentiviral construct demonstrated as percentage of GFP or NaKtide transduced cells, N=9-14/group. (C) NaKtide concentration in visceral adipose assessed by competitive ELISA, n=6/group. (D) TBARS, N=6/group; (E) protein carbonylation, N=5/group; (F) pSrc normalized to total Src, N=8/group. mRNA expression of (G) TLR4, N=6/group; (H) TRAF6, N=6/group. Each box and whisker plot represent values as maximum and minimum range, upper quartile, median and lower quartile. *$p < 0.05$ vs. Sham, **$p < 0.01$ vs. Sham, #$p < 0.05$ vs. PNx, ##$p < 0.01$ vs. PNx, &$p < 0.05$ vs. PNx+WD, &&$p < 0.01$ vs. PNx+WD.

mice fed a WD showed significantly upregulated expression of phosphorylated-Src (p-Src), as compared to PNx mice (Fig. 1F). Notably, the increase in the expression of p-Src was significantly attenuated by adipo-NaKtide in PNx and PNx+WD mice (Fig. 1F). Our results further showed significantly upregulated mRNA expression of the Na, K-ATPase signaling downstream mediators, TLR4 and TRAF6 in adipose tissue of PNx and PNx+WD mice compared to Sham (Fig. 1G and H). Adipocyte-specific transduction of NaKtide attenuated levels of both in PNx and PNx+WD mice (Fig. 1G and H).

Adipo-NaKtide improves mitochondrial biogenesis, attenuates inflammation and apoptosis in adipose tissue of PNx mice

While impaired mitochondrial function in adipocytes has been known to occur in altered oxidative stress, PGC-1α and Sirt3 are well-established markers that mediate mitochondrial biogenesis and function (39). Our result showed a significant reduction of PGC-1α mRNA expression in the adipose tissue of PNx and PNx+WD mice compared to Sham (Fig. 2A and B). The transduction of adipo-NaKtide significantly increased the expression of PGC-1α and Sirt3 mRNA expression, suggesting that the NaKtide improved mitochondrial function (Fig. 2A and B). Our results also showed significant upregulation of inflammatory cytokines, IL-6, TNFα and leptin in the adipose tissue of WD-fed PNx mice, as compared to Sham (Fig. 2C-E). Adipo-NaKtide attenuated the increase in the expression of these inflammatory cytokines in the adipose tissue of WD-fed PNx mice (Fig. 2C-E). Our results also showed adipo-NaKtide decreased the expression of F4/80, a marker of macrophage infiltration, which was upregulated by PNx and PNx+WD (Fig. 2F). The dysregulation of mitochondrial function and inflammation in the adipocyte are intricately linked to cellular apoptosis. Accordingly, our results showed a significant increase in the expression of apoptotic markers, Casp9 and Bax in the adipose tissue of PNx+WD mice, as compared to Sham and PNx alone (Fig. 2G and H). The transduction of adipo-NaKtide caused a marked reduction in the elevated expression of these apoptotic markers (Fig. 2G and H).

Adipo-NaKtide improves glucose tolerance and systemic inflammation in PNx mice

Mice with experimental uremic cardiomyopathy induced by PNx showed impaired glucose tolerance, suggestive of insulin resistance, which was exacerbated by the WD regimen (Fig. 3A). Transduction of adipo-NaKtide improved glucose tolerance in these mice (Fig. 3A). To study the effects of adipo-NaKtide on systemic oxidative stress, we measured the plasma levels of inflammatory cytokines. Our results showed a significant increase in systemic inflammation, demonstrated by higher levels of IL-6, MCP1 and TNFα, in PNx mice which was further aggravated in PNx+WD, as compared to PNx (Fig. 3B-D). The increase in the levels of these inflammatory cytokines was attenuated by adipo-NaKtide in PNx and PNx+WD mice (Fig. 3B-D). In addition, adipo-NaKtide also significantly attenuated the increased levels of plasma leptin in PNx+WD mice (Fig. 3E). Collectively, our results demonstrate transduction of adipocyte-specific NaKtide in PNx mice improved oxidative stress conducive to systemic inflammation.

As expected, our results showed that PNx mice, had significantly increased levels of plasma creatinine, more so in PNx+WD mice (Fig. 3F). Adipo-NaKtide attenuated plasma creatinine levels in PNx+WD mice (Fig. 3F). The accumulation of putative uremic toxins is a hallmark of experimental uremia, which is also causative of oxidative stress. Our results showed significantly elevated plasma levels of uremic toxin, indoxyl sulfate, in PNx and PNx+WD mice (Fig. 3G). Conversely, determination of hematocrit showed a significant reduction in PNx and PNx+WD mice, as compared to Sham, which was improved by adipo-NaKtide (Fig. 3H).

Adipo-NaKtide improves cardiac phenotype in mice with PNx-induced experimental uremic cardiomyopathy

Our results showed that the heart weight was significantly higher in the PNx and PNx+WD mice as compared
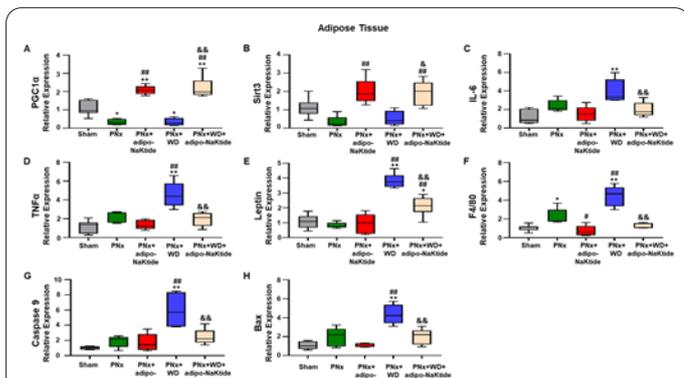
Figure 2. Adipo-NaKtide improves mitochondrial function, attenuates inflammation and apoptosis in visceral adipose tissue of PNx mice. mRNA expression of (A) PGC1α, N=4-7/group; (B) Sirt3, N=4-7/group; (C) IL-6, N=5-7/group; (D) TNFα, N=5-7/group; (E) Leptin, N=5-7/group; (F) F4/80, N=5-7/group; (G) Caspase9, N=5-6/group and (H) Bax, N=5-6/group. Each box and whisker plot represents values as maximum and minimum range, upper quartile, median and lower quartile. *p < 0.05 vs. Sham, **p < 0.01 vs. Sham, #p < 0.05 vs. PNx, ##p < 0.01 vs. PNx, &p < 0.05 vs. PNx+WD, &&p < 0.01 vs. PNx+WD.
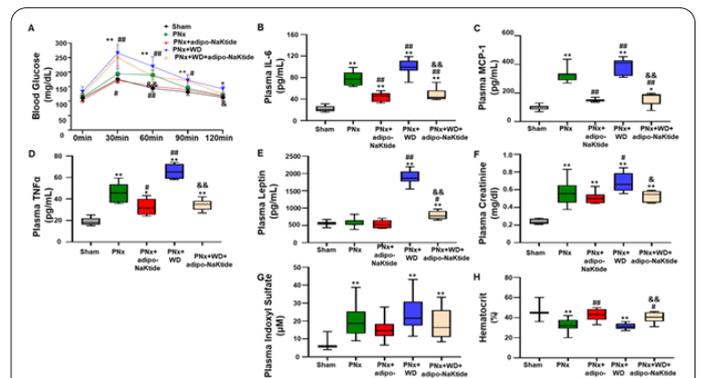
Figure 3. Adipo-NaKtide improves glucose tolerance and systemic inflammation in PNx mice. (A) Glucose tolerance test, N=8-12/group. Plasma concentrations of (B) IL-6, N= 6-12/group; (C) MCP-1, n=5-16/group; (D) TNFα, N=6/group and (E) Leptin, N=6-12/group. Plasma (F) creatinine, N=6-16/group and (G) indoxyl sulfate concentrations, N=12/group. (H) Hematocrit, N=6-24/group. Each box and whisker plot represents values as maximum and minimum range, upper quartile, median and lower quartile. *p < 0.05 vs. Sham, **p < 0.01 vs. Sham, #p < 0.05 vs. PNx, ##p < 0.01 vs. PNx, &p < 0.05 vs. PNx+WD, &&p < 0.01 vs. PNx+WD

to Sham (Fig. 4A). Transduction with adipo-NaKtide prevented these increases in these mice (Fig. 4A). These results were confirmed by echocardiography (Table 1). Histological staining provided evidence of increased cardiac fibrosis in PNx mice, which was further worsened by WD. Notably, treatment with adipo-NaKtide attenuated the increased cardiac fibrosis in the PNx mouse model (Fig. 4B). In addition to the effects on cardiac fibrosis, NaKtide targeted specifically to adipocytes attenuated expression of inflammatory markers, TNFα and IL-6 in the cardiac tissue of PNx and PNx+WD mice (Fig. 4C and D). The mRNA expression of collagen 1 also increased in PNx and PNx+WD mice as compared to Sham, but were improved by adipo-NaKtide transduction (Fig. 4E). Conversely, expression of Fli-1 was reversed by adipo-NaKtide, which was significantly reduced in PNx+WD (Fig. 4F). Our results also showed that protein carbonylation was increased in the PNx group, as compared to Sham, which was further exacerbated by concurrent WD (Fig. 4G). Transduction of adipo-NaKtide attenuated protein carbonylation in cardiac tissue of these mice with PNx and PNx+WD (Fig. 4G).

Effect of adipocyte-specific sNaKtide and skeletal muscle-specific NaKtide on systemic inflammation and cardiac phenotype in PNx mice

To serve as a control for NaKtide expression, PNx mice were transduced with adipocyte-specific sNaKtide. Our results confirmed that adipo-sNaKtide does not affect p-Src expression, as the upregulation of pSrc in visceral adipose tissue of PNx mice was not attenuated by adipo-sNaKtide (Fig. S3). This was contrary to the effect of adi-po-NaKtide which significantly attenuated pSrc expression in PNx mice. To confirm that Na, K-ATPase signaling in adipocytes plays a role in uremic cardiomyopathy and to serve as a control for adipocyte-specific expression of NaKtide, we transduced NaKtide in PNx mice using a lentiviral construct with myoD promoter, to target NaKtide
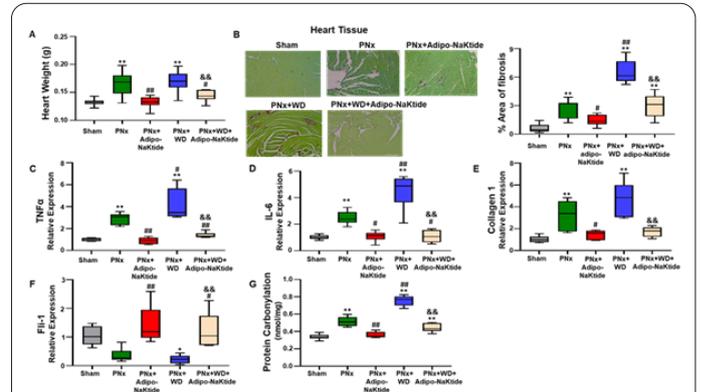
Figure 4. **Adipo-NaKtide improves cardiac phenotype in PNx mice.** (A) Heart weight, N=6-24/group (B) Representative images and quantification for cardiac fibrosis assessed with Sirius red staining. Images were taken with 20X objective lens; scale bar represents 100μm, N=6-12/group. mRNA expression of (C) TNFα, N=6/group; (D) IL-6, N=6/group; (E) Collagen 1, N=6/group and (F) Fli-1, N=5-6/group. (G) Protein carbonylation levels, N=6/group. Each box and whisker plot represents values as maximum and minimum range, upper quartile, median and lower quartile. *p < 0.05 vs. Sham, **p < 0.01 vs. Sham, #p < 0.05 vs. PNx, ##p < 0.01 vs. PNx, &p < 0.05 vs. PNx+WD, &&p < 0.01 vs. PNx+WD.

Table 1. Summary of weights and transthoracic echocardiograph results.

	Sham (N=8-12)	PNx (N=11-24)	PNx+adipo-NaKtide (N=12-13)	PNx+WD (N=8-15)	PNx+WD+adipo-NaKtide (N=6-9)
Weights					
Body Weight (g)	27.1 ± 0.5	27.9 ± 0.5	26.2 ± 0.5	28.0 ± 0.8	29.3 ± 0.9
Visceral Fat (g)	0.54 ± 0.08	0.49 ± 0.07	0.48 ± 0.09	0.59 ± 0.08	0.63 ± 0.11
Heart Weight (g)	0.132±0.002	0.164±0.004**	0.132±0.003^^	0.170±0.004**	0.144±0.004^^##
Echocardiography					
ESA, mm2	16.4 ± 0.6	17.4 ± 0.8	15.3 ± 0.7	19.6 ± 0.5	16.6 ± 0.7
ESD, mm	3.12 ± 0.14	3.35 ± 0.07	3.18 ± 0.04	3.65 ± 0.06**	3.19 ± 0.07##
PWT, mm	0.52 ± 0.02	0.64 ± 0.01**	0.57 ± 0.01^^	0.64 ± 0.02**	0.58 ± 0.01^^##
AWT, mm	0.61 ± 0.01	0.73 ± 0.01**	0.63 ± 0.01^^	0.73 ± 0.01**	0.65 ± 0.01^^##
IVCT+IVRT, msec	17.0 ± 0.5	24.5 ± 0.7**	16.8 ± 0.5^^	21.8 ± 0.8**^	17.6 ± 0.8^^##
PaVTI, mm	27.8 ± 0.9	28.2 ± 0.9	29.8 ± 0.5	25.4 ± 0.7	28.5 ± 0.4
PaD, mm	0.96 ± 0.02	1.02 ± 0.02*	0.97 ± 0.01^	0.93 ± 0.01^^	1.04 ± 0.01*##
RWT	0.25 ± 0.007	0.31 ± 0.003**	0.27 ± 0.002**^^	0.31 ± 0.004**	0.27 ± 0.004**^^##
MPI	0.42 ± 0.02	0.57 ± 0.02**	0.38 ± 0.01^^	0.57 ± 0.02**	0.41 ± 0.02^^##
FS, %	29.9 ± 2.3	23.8 ± 1.0*	26.9 ± 0.7	16.0 ± 0.8**^^	27.7 ± 1.0##
EF, %	64.7 ± 3.2	55.6 ± 1.7*	60.8 ± 1.0	40.6 ± 1.7**^^	62.0 ± 1.6##
CO, ml/min	9.2 ± 0.5	9.8 ± 0.3	9.5 ± 0.3	8.4 ± 0.4^	11.0 ± 0.4##
LVM, mg	90 ± 2	112 ± 3**	94 ± 3^^	110 ± 3**	98 ± 3^^##
LVMI	3.40 ± 0.11	4.17 ± 0.11**	3.65 ± 0.10^^	4.01 ± 0.14*	3.47 ± 0.18^^##

Each column shows the mean ± SEM for the 5 experimental groups. ESA, end systolic area; ESD, end systolic dimension; PWT, posterior wall thickness; AWT, anterior wall thickness; IVCT, isovolumic contraction time; IVRT, isovolumic relaxation time; PaVTI, pulmonary artery velocity time integral; PaD, pulmonary artery dimension; RWT, relative wall thickness; MPI, myocardial performance index; FS, fractional shortening; EF, ejection fraction; CO, cardiac .

output; LVM, left ventricular mass; LVMI, left ventricular mass index. * p<0.05, **p<0.01 vs. Sham; ^p<0.05, ^^ p<0.01 vs PNx; # p<0.05, ## p<0.01 vs PNx+WD.

expression in skeletal muscles. We chose skeletal muscle because the amount of this tissue was comparable to that of the adipocyte mass (40). Immunofluorescence staining of mice transduced with myoD-NaKtide showed readily detectable expression of green fluorescence (GFP) and red fluorescence (NaKtide), specifically in skeletal muscle tissue, while there was no notable expression in adipose and heart tissues (Fig. S4A). To further confirm the presence of NaKtide, competitive ELISA performed on skeletal muscle tissue showed high concentrations of NaKtide in myoD-NaKtide transduced Sham and PNx mice, while levels of NaKtide were undetectable in mice transduced with myoD-GFP only (Fig. S4B). PNx mice showed a significant increase in heart weight, as compared to Sham, which was reverted by adipo-NaKtide, while adipo-sNaKtide and myoD-NaKtide showed no effect on the heart weight of these mice (Fig. 5A). Also, adipo-sNaKtide did not alter the cardiac function and morphology as depicted in Supplemental Table 1. Plasma creatinine was increased in all PNx and lentivirus transduced PNx mice, as compared to Sham (Fig. 5B). Adipo-NaKtide transduced PNx mice showed improved hematocrit levels, as compared to PNx (Fig. 5C). Transduction of adipo-sNaKtide and myoD-NaKtide in PNx did not improve hematocrit level (Fig. 5C). Furthermore, adipo-sNaKtide and myoD-NaKtide did not attenuate systemic inflammation in PNx, as assessed by levels of plasma TNFα and MCP1 (Fig. 5D and E). Our results also showed that, unlike adipo-NaKtide, transduction of adipo-sNaKtide and myoD-NaKtide in PNx mice failed to attenuate the expression of cardiac inflammation, as assessed by cardiac IL-6 and TNFα (Fig. 5F and G), as well as cardiac fibrosis, assessed by expression of collagen 1 (Fig. 5H).

Effect on renal function, systemic inflammation and cardiac function in 4/6-nephrectomy mice

We aimed to compare the effect of adipo-NaKtide transduction in PNx with a milder model of renal failure, in mice with 4/6-nephrectomy, to demonstrate that improvement in experimental uremic cardiomyopathy is induced by antagonism of Na, K-ATPase signaling specifically in adipocytes. Our results showed a significant increase in levels of plasma creatinine and plasma cystatin C, which are well-known markers of renal dysfunction, in PNx mice, however, the extent of these increases was lower in mice with 4/6-nephrectomy (Fig. 6A and B). PNx mice had significantly lower levels of hematocrit, when compared to 4/6-nephrectomy mice and adipo-NaKtide transduced mice (Fig. 6C). However, systemic evidence of inflammation, assessed by plasma levels of TNFα and MCP-1, was demonstrably worse in 4/6-nephrectomy mice as compared to adipo-NaKtide transduced PNx mice (Fig. 6D and E). Heart weight was significantly higher in PNx, as compared to Sham and 4/6-nephrectomy mice (Fig. 6F). Mice with 4/6-nephrectomy had lower protein carbonylation levels, as compared to PNx (Fig. 6G). However, adipo-NaKtide further attenuated protein carbonylation levels, more so than 4/6-nephrectomy mice (Fig. 6G).

Effect on cardiac fibrosis and cardiac function in 4/6-nephrectomy mice

Morphological assessment of cardiac tissue showed significantly high cardiac fibrosis in PNx and 4/6-nephrectomy mice, as compared to Sham, however, cardiac fibrosis
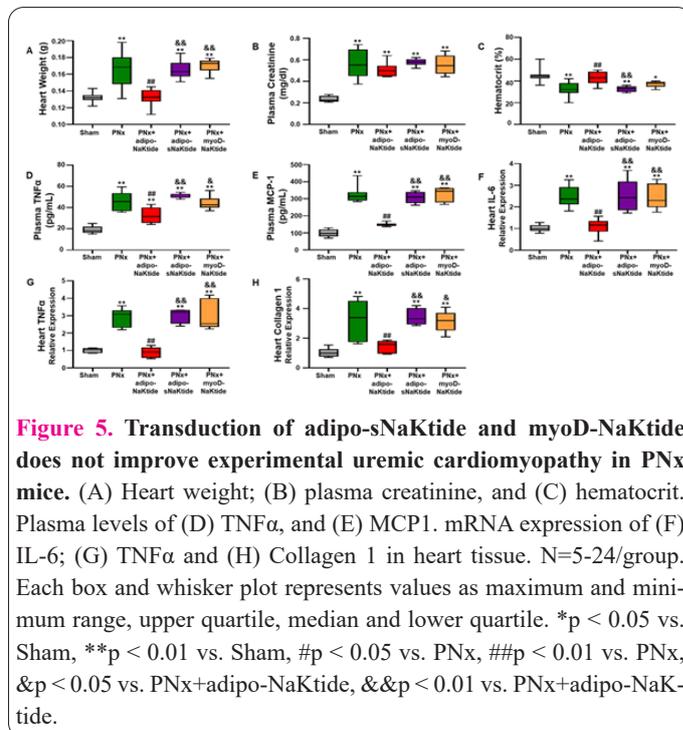
Figure 5. **Transduction of adipo-sNaKtide and myoD-NaKtide does not improve experimental uremic cardiomyopathy in PNx mice.** (A) Heart weight; (B) plasma creatinine, and (C) hematocrit. Plasma levels of (D) TNFα, and (E) MCP1. mRNA expression of (F) IL-6; (G) TNFα and (H) Collagen 1 in heart tissue. N=5-24/group. Each box and whisker plot represents values as maximum and minimum range, upper quartile, median and lower quartile. *p < 0.05 vs. Sham, **p < 0.01 vs. Sham, #p < 0.05 vs. PNx, ##p < 0.01 vs. PNx, &p < 0.05 vs. PNx+adipo-NaKtide, &&p < 0.01 vs. PNx+adipo-NaKtide.
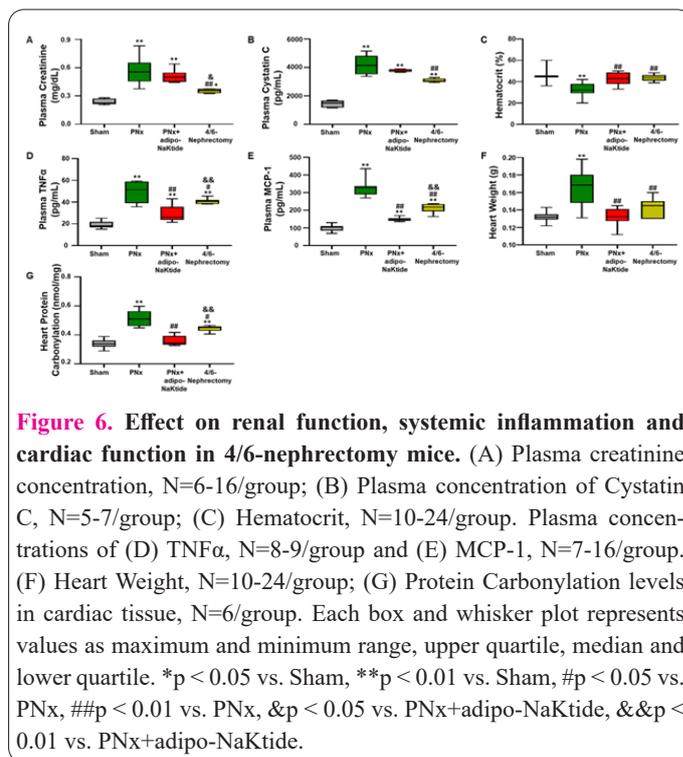
Figure 6. **Effect on renal function, systemic inflammation and cardiac function in 4/6-nephrectomy mice.** (A) Plasma creatinine concentration, N=6-16/group; (B) Plasma concentration of Cystatin C, N=5-7/group; (C) Hematocrit, N=10-24/group. Plasma concentrations of (D) TNFα, N=8-9/group and (E) MCP-1, N=7-16/group. (F) Heart Weight, N=10-24/group; (G) Protein Carbonylation levels in cardiac tissue, N=6/group. Each box and whisker plot represents values as maximum and minimum range, upper quartile, median and lower quartile. *p < 0.05 vs. Sham, **p < 0.01 vs. Sham, #p < 0.05 vs. PNx, ##p < 0.01 vs. PNx, &p < 0.05 vs. PNx+adipo-NaKtide, &&p < 0.01 vs. PNx+adipo-NaKtide.

was improved by adipo-NaKtide (Fig. 7A). Cardiac function was assessed by echocardiography in 4/6-nephrectomy mice (Table S2). We found abnormal cardiac function in 4/6-nephrectomy; however, the extent was lower than PNx. The expression of the inflammatory marker, TNFα, in cardiac tissue of 4/6-nephrectomy mice, was lower as compared to PNx, but significantly higher than adipo-NaKtide transduced PNx mice (Fig. 7B). Subsequently, expression of the inflammatory marker, IL-6, was significantly higher in PNx and 4/6-nephrectomy mice compared to sham, which was attenuated by adipo-NaKtide (Fig. 7C). The mRNA expression of collagen 1 also increased in PNx and 4/6-nephrectomy mice, but was improved by adipo-NaKtide transduction (Fig. 7D). Conversely, expression of Fli-1 was reversed by adipo-NaKtide, which was reduced in PNx and 4/6-nephrectomy mice (Fig. 7E).

Figure 7. Effect on cardiac fibrosis and cardiac function in 4/6-nephrectomy mice. (A) Representative images and quantification of cardiac fibrosis (N=8-12/group). Images were taken with a 20X objective lens; the scale bar represents 100µm. mRNA expression of (B) TNFα, N=6-8/group; (C) IL-6, N=6-8/group; (D) Collagen 1, N=6/group and (E) Fli-1, N=6/group. Each box and whisker plot represents values as maximum and minimum range, upper quartile, median and lower quartile. *p < 0.05 vs. Sham, **p < 0.01 vs. Sham, #p < 0.05 vs. PNx, ##p < 0.01 vs. PNx, &p < 0.05 vs. PNx+adipo-NaKtide, &&p < 0.01 vs. PNx+adipo-NaKtide.

Discussion

Uremic cardiomyopathy is an intricate and multifactorial pathological cardiac hypertrophy that accompanies advanced chronic kidney disease. It poses a significant burden in end-stage renal disease patients with a high morbidity and mortality rate (27, 41-43). The pathophysiology of uremic cardiomyopathy involves a complex interplay of a multitude of traditional cardiovascular risk factors along with systemic oxidative stress which is ubiquitous in advanced chronic renal failure (41). Mounting evidence suggests that interactions and crosstalk between the different signaling pathways that involve derangements of cellular redox status is apparent in uremic cardiomyopathy (44-46).

We have previously reported that systemic administration of pNaKtide can attenuate oxidant stress and ameliorate experimental uremic cardiomyopathy induced by partial nephrectomy (27). The study showed that signaling through the Na/K-ATPase produces oxidative stress that recruits inflammation and further exacerbates the pathophysiology of uremic cardiomyopathy. The present study demonstrates the specific role of adipocytes in the pathogenesis and progression of uremic cardiomyopathy. Here in this study, we administrated WD (high fat and high fructose) for activating NKAL and adipocyte-specific expression of NaKtide was utilized to antagonize the NKAL. We observed a phenotypical difference in PNx mice supplemented with WD when compared to the ones without renal failure, especially in the case of weight gain. Our results showed that adipocyte-specific NaKtide expression could significantly attenuate the dysregulation in the adipocyte inflammatory status and systemic cytokine concentration in experimental uremic cardiomyopathy and essentially prevented the progression of uremic cardiomyopathy in the animals with PNx. However, administration of either a lentivirus using a muscle-specific promoter to drive NaKtide expression or an adipocyte-specific expression of a sNaKtide both had no apparent effects on the pathophysiological changes of uremic cardiomyopathy.

NaKtide could significantly modulate the inflammatory and apoptotic signaling pathways in adipose tissue which

in turn improved glucose tolerance, systemic inflammation and anemia in experimental uremic cardiomyopathy. The improved cardiac phenotype and function, evidenced by the observations of cardiac fibrosis and echo measurements, reinforced our findings. Our study demonstrates that the improved adipocyte phenotype in adipo-NaKtide transduced mice resulted in the modulation of systemic inflammatory status which can be either through direct suppression of inflammatory cytokines by the adipo-NaKtide vector or by intermediary agents that link the progression of uremic cardiomyopathy. Accumulating evidence shows the role of adipocyte-derived exosomes in the activation of inflammatory signaling and in the inter-organ communication that contributes to various metabolic diseases (47, 48). Of note, adipocytes are associated with the pro-inflammatory comorbidities of uremia (49-51). Thus, adipokine dysregulation and adipocyte-derived exosomes can furnish systemic inflammatory cytokines as seen in PNx and PNx + WD. So, the modulation of systemic oxidative stress in the uremic milieu and the observed beneficial effect in the experimental uremic cardiomyopathy can be because of the adipocyte-specific antagonism of NKAL by NaKtide.

To conclude, our findings demonstrate the promising role of adipocyte NKAL in the attenuation of systemic manifestations of uremic cardiomyopathy. Even though the blockade of NKAL exhibited potential amelioration of the inflammatory phenotype in experimental uremia, other intervention strategies that attenuate oxidant stress may also provide approaches for improved clinical applications. The present findings will aid the future understanding of the detailed molecular mechanism behind the specific role of adipocyte and adipocyte NKAL in the progression of uremic cardiomyopathy and if these data are confirmed in humans, it may contribute to the development of novel targets for therapeutic intervention.

The key innovation of the study lies in the central hypothesis that Na/K-ATPase signaling in adipocytes contributes to the development of uremic cardiomyopathy. In the present study, we have used a novel adipocyte-specific NaKtide lentivirus construct. This construct has ensured the adipocyte-specific effects as well as limited off-target effects. To the best of our knowledge, the role of adipocytes in the development and maintenance of uremic cardiomyopathy has never been explored, and if proven, produces a therapeutic target for uremic cardiomyopathy and other diseases.

Authors Contributions

Komal Sodhi: Designed the experiments, and wrote the manuscript; Xiaoliang Wang: Performed the experiments; M. Aslam Chaudhary: Performed the experiments; Hari Vishal Lakhani: Performed the experiments; Mishghan Zehra: Performed the experiments; Athar Nawab: Performed the experiments; Cameron L. Cottrill: Performed the experiments; Fang Bai: Performed the experiments; Jiang Liu: Performed the experiments; Juan R. Sanabria: Edited the manuscript; Zijian Xie: Edited the manuscript. Unfortunately, Dr. Xie passed away during the construction of the revised manuscript. We will miss him very much; Joseph I. Shapiro: Designed the overall project as well as individual experiments, analyzed data and served as senior author in the writing of the manuscript

Competing Interests

All authors declare no competing interests.

Data and materials availability

All data is available in the main text or the supplementary materials.

References

1. Koenen M, Hill MA, Cohen P, Sowers JR. Obesity, Adipose Tissue and Vascular Dysfunction. Circ Res. 2021 Apr 2;128(7):951-968. doi: 10.1161/CIRCRESAHA.121.318093.

2. Chait A, den Hartigh LJ. Adipose Tissue Distribution, Inflammation and Its Metabolic Consequences, Including Diabetes and Cardiovascular Disease. Front Cardiovasc Med. 2020 Feb 25;7:22. doi: 10.3389/fcvm.2020.00022.

3. Saponaro C, Sabatini S, Gaggini M, Carli F, Rosso C, Positano V, et al. Adipose tissue dysfunction and visceral fat are associated with hepatic insulin resistance and severity of NASH even in lean individuals. Liver Int. 2022 Nov;42(11):2418-2427. doi: 10.1111/liv.15377.

4. Maslov LN, Naryzhnaya NV, Boshchenko AA, Popov SV, Ivanov VV, Oeltgen PR. Is oxidative stress of adipocytes a cause or a consequence of the metabolic syndrome? J Clin Transl Endocrinol. 2018 Nov 9;15:1-5. doi: 10.1016/j.jcte.2018.11.001.

5. Furukawa S, Fujita T, Shimabukuro M, Iwaki M, Yamada Y, Nakajima Y, et al. Increased oxidative stress in obesity and its impact on metabolic syndrome. J Clin Invest. 2004 Dec;114(12):1752-61. doi: 10.1172/JCI21625.

6. Hauck AK, Huang Y, Hertzel AV, Bernlohr DA. Adipose oxidative stress and protein carbonylation. J Biol Chem. 2019 Jan 25;294(4):1083-1088. doi: 10.1074/jbc.R118.003214.

7. Le Lay S, Simard G, Martinez MC, Andriantsitohaina R. Oxidative stress and metabolic pathologies: from an adipocentric point of view. Oxid Med Cell Longev. 2014;2014:908539. doi: 10.1155/2014/908539

8. Xu H, Barnes GT, Yang Q, Tan G, Yang D, Chou CJ, et al. Chronic inflammation in fat plays a crucial role in the development of obesity-related insulin resistance. J Clin Invest. 2003 Dec;112(12):1821-30. doi: 10.1172/JCI19451.

9. Weisberg SP, McCann D, Desai M, Rosenbaum M, Leibel RL, Ferrante AW, Jr. Obesity is associated with macrophage accumulation in adipose tissue. J Clin Invest. 2003 Dec;112(12):1796-808. doi: 10.1172/JCI19246.

10. Oberg BP, McMenamin E, Lucas FL, McMonagle E, Morrow J, Ikizler TA, et al. Increased prevalence of oxidant stress and inflammation in patients with moderate to severe chronic kidney disease. Kidney Int. 2004 Mar;65(3):1009-16. doi: 10.1111/j.1523-1755.2004.00465.x.

11. London GM, Parfrey PS. Cardiac disease in chronic uremia: pathogenesis. Adv Ren Replace Ther. 1997 Jul;4(3):194-211. doi: 10.1016/s1073-4449(97)70029-3.

12. D'Agostino M, Mauro D, Zicarelli M, Carullo N, Greco M, Andreucci M, et al. miRNAs in Uremic Cardiomyopathy: A Comprehensive Review. Int J Mol Sci. 2023 Mar 12;24(6):5425. doi: 10.3390/ijms24065425.

13. Pieniazek A, Bernasinska-Slomczewska J, Gwozdzinski L. Uremic Toxins and Their Relation with Oxidative Stress Induced in Patients with CKD. Int J Mol Sci. 2021 Jun 8;22(12):6196. doi: 10.3390/ijms22126196.

14. de Albuquerque Suassuna PG, Sanders-Pinheiro H, de Paula RB. Uremic Cardiomyopathy: A New Piece in the Chronic Kidney Disease-Mineral and Bone Disorder Puzzle. Front Med (Lausanne). 2018 Jul 24;5:206. doi: 10.3389/fmed.2018.00206.

15. Rossi M, Campbell KL, Johnson DW, Stanton T, Vesey DA, Coombes JS, et al. Protein-bound uremic toxins, inflammation and oxidative stress: a cross-sectional study in stage 3-4 chronic kidney disease. Arch Med Res. 2014 May;45(4):309-17. doi: 10.1016/j.arcmed.2014.04.002.

16. Liang M, Tian J, Liu L, Pierre S, Liu J, Shapiro J, et al. Identification of a pool of non-pumping Na/K-ATPase. J Biol Chem. 2007 Apr 6;282(14):10585-93. doi: 10.1074/jbc.M609181200.

17. Yan Y, Haller S, Shapiro A, Malhotra N, Tian J, Xie Z, et al. Ouabain-stimulated trafficking regulation of the Na/K-ATPase and NHE3 in renal proximal tubule cells. Mol Cell Biochem. 2012 Aug;367(1-2):175-83. doi: 10.1007/s11010-012-1331-x.

18. Liu J, Yan Y, Liu L, Xie Z, Malhotra D, Joe B, et al. Impairment of Na/K-ATPase signaling in renal proximal tubule contributes to Dahl salt-sensitive hypertension. J Biol Chem. 2011 Jul 1;286(26):22806-13. doi: 10.1074/jbc.M111.246249.

19. Liu J, Liang M, Liu L, Malhotra D, Xie Z, Shapiro JI. Ouabain-induced endocytosis of the plasmalemmal Na/K-ATPase in LLC-PK1 cells requires caveolin-1. Kidney Int. 2005 May;67(5):1844-54. doi: 10.1111/j.1523-1755.2005.00283.x.

20. Liu J. Ouabain-induced endocytosis and signal transduction of the Na/K-ATPase. Front Biosci. 2005 Sep 1;10:2056-63. doi: 10.2741/1681.

21. Liu J, Kesiry R, Periyasamy SM, Malhotra D, Xie Z, Shapiro JI. Ouabain induces endocytosis of plasmalemmal Na/K-ATPase in LLC-PK1 cells by a clathrin-dependent mechanism. Kidney Int. 2004 Jul;66(1):227-41. doi: 10.1111/j.1523-1755.2004.00723.x.

22. Liu J, Tian J, Haas M, Shapiro JI, Askari A, Xie Z. Ouabain interaction with cardiac Na+/K+-ATPase initiates signal cascades independent of changes in intracellular Na+ and Ca2+ concentrations. J Biol Chem. 2000 Sep 8;275(36):27838-44. doi: 10.1074/jbc.M002950200.

23. Yan Y, Shapiro AP, Haller S, Katragadda V, Liu L, Tian J, et al. Involvement of reactive oxygen species in a feed-forward mechanism of Na/K-ATPase-mediated signaling transduction. J Biol Chem. 2013 Nov 22;288(47):34249-34258. doi: 10.1074/jbc.M113.461020.

24. Wang Y, Ye Q, Liu C, Xie JX, Yan Y, Lai F, et al. Involvement of Na/K-ATPase in hydrogen peroxide-induced activation of the Src/ERK pathway in LLC-PK1 cells. Free Radic Biol Med. 2014 Jun;71:415-426. doi: 10.1016/j.freeradbiomed.2014.03.036.

25. Srikanthan K, Shapiro JI, Sodhi K. The Role of Na/K-ATPase Signaling in Oxidative Stress Related to Obesity and Cardiovascular Disease. Molecules. 2016 Sep 3;21(9):1172. doi: 10.3390/molecules21091172.

26. Li Z, Cai T, Tian J, Xie JX, Zhao X, Liu L, et al. NaKtide, a Na/K-ATPase-derived peptide Src inhibitor, antagonizes ouabain-activated signal transduction in cultured cells. J Biol Chem. 2009 Jul 31;284(31):21066-76. doi: 10.1074/jbc.M109.013821.

27. Liu J, Tian J, Chaudhry M, Maxwell K, Yan Y, Wang X, et al. Attenuation of Na/K-ATPase Mediated Oxidant Amplification with pNaKtide Ameliorates Experimental Uremic Cardiomyopathy.

Sci Rep. 2016 Oct 4;6:34592. doi: 10.1038/srep34592.

28. Li H, Yin A, Cheng Z, Feng M, Zhang H, Xu J, et al. Attenuation of Na/K-ATPase/Src/ROS amplification signal pathway with pNaktide ameliorates myocardial ischemia-reperfusion injury. Int J Biol Macromol. 2018 Oct 15;118(Pt A):1142-1148. doi: 10.1016/j.ijbiomac.2018.07.001.

29. Hangaard L, Bouzinova EV, Staehr C, Dam VS, Kim S, Xie Z, et al. Na-K-ATPase regulates intercellular communication in the vascular wall via cSrc kinase-dependent connexin43 phosphorylation. Am J Physiol Cell Physiol. 2017 Apr 1;312(4):C385-C397. doi: 10.1152/ajpcell.00347.2016.

30. Cheng X, Song Y, Wang Y. pNaKtide ameliorates renal interstitial fibrosis through inhibition of sodium-potassium adenosine triphosphatase-mediated signaling pathways in unilateral ureteral obstruction mice. Nephrol Dial Transplant. 2019 Feb 1;34(2):242-252. doi: 10.1093/ndt/gfy107.

31. Munis AM. Gene Therapy Applications of Non-Human Lentiviral Vectors. Viruses. 2020 Sep 29;12(10):1106. doi: 10.3390/v12101106.

32. Wu W, Zhang J, Zhao C, Sun Y, Yin Y, Peng Y, et al. Lentivirus-mediated CTRP6 silencing ameliorates diet-induced obesity in mice. Exp Cell Res. 2018 Jun 1;367(1):15-23. doi: 10.1016/j.yexcr.2018.01.027.

33. Eerola K, Nordlund W, Virtanen S, Dickens AM, Mattila M, Ruohonen ST, et al. Lentivirus-mediated alpha-melanocyte-stimulating hormone overexpression in the hypothalamus decreases diet induced obesity in mice. J Neuroendocrinol. 2013 Dec;25(12):1298-1307. doi: 10.1111/jne.12109.

34. Cao J, Sodhi K, Inoue K, Quilley J, Rezzani R, Rodella L, et al. Lentiviral-human heme oxygenase targeting endothelium improved vascular function in angiotensin II animal model of hypertension. Hum Gene Ther. 2011 Mar;22(3):271-82. doi: 10.1089/hum.2010.059.

35. Bian J, Bai XM, Zhao YL, Zhang L, Liu ZJ. Lentiviral vector-mediated knockdown of Lrb in the arcuate nucleus promotes diet-induced obesity in rats. J Mol Endocrinol. 2013 May 17;51(1):27-35. doi: 10.1530/JME-12-0212.

36. Ames RS, Lu Q. Viral-mediated gene delivery for cell-based assays in drug discovery. Expert Opin Drug Discov. 2009 Mar;4(3):243-56. doi: 10.1517/17460440902751599.

37. Haller ST, Kennedy DJ, Shidyak A, Budny GV, Malhotra D, Fedorova OV, et al. Monoclonal antibody against marinobufagenin reverses cardiac fibrosis in rats with chronic renal failure. Am J Hypertens. 2012 Jun;25(6):690-6. doi: 10.1038/ajh.2012.17.

38. Handala L, Fiore T, Rouille Y, Helle F. QuantIF: An ImageJ Macro to Automatically Determine the Percentage of Infected Cells after Immunofluorescence. Viruses. 2019 Feb 19;11(2):165. doi: 10.3390/v11020165.

39. Kong X, Wang R, Xue Y, Liu X, Zhang H, Chen Y, et al. Sirtuin 3, a new target of PGC-1alpha, plays an important role in the suppression of ROS and mitochondrial biogenesis. PLoS One. 2010 Jul 22;5(7):e11707. doi: 10.1371/journal.pone.0011707.

40. Gallagher D, Kuznia P, Heshka S, Albu J, Heymsfield SB, Goodpaster B, et al. Adipose tissue in muscle: a novel depot similar in size to visceral adipose tissue. Am J Clin Nutr. 2005 Apr;81(4):903-10. doi: 10.1093/ajcn/81.4.903.

41. Wang X, Shapiro JI. Evolving concepts in the pathogenesis of uraemic cardiomyopathy. Nat Rev Nephrol. 2019 Mar;15(3):159-175. doi: 10.1038/s41581-018-0101-8.

42. Drummond CA, Buddny G, Haller ST, Liu J, Yan Y, Xie Z, et al. Gender differences in the development of uremic cardiomyopathy following partial nephrectomy: Role of progesterone. J Hypertens (Los Angel). 2013 Jan 31;2:10.4172/2167-1095.1000109. doi: 10.4172/2167-1095.1000109.

43. Garikapati K, Goh D, Khanna S, Echampati K. Uraemic Cardiomyopathy: A Review of Current Literature. Clin Med Insights Cardiol. 2021 Feb 23;15:1179546821998347. doi: 10.1177/1179546821998347.

44. Wang X, Liu J, Drummond CA, Shapiro JI. Sodium potassium adenosine triphosphatase (Na/K-ATPase) as a therapeutic target for uremic cardiomyopathy. Expert Opin Ther Targets. 2017 May;21(5):531-541. doi: 10.1080/14728222.2017.1311864.

45. Kennedy DJ, Malhotra D, Shapiro JI. Molecular insights into uremic cardiomyopathy: cardiotonic steroids and Na/K ATPase signaling. Cell Mol Biol (Noisy-le-grand). 2006 Dec 30;52(8):3-14.

46. Taylor D, Bhandari S, Seymour AM. Mitochondrial dysfunction in uremic cardiomyopathy. Am J Physiol Renal Physiol. 2015 Mar 15;308(6):F579-87. doi: 10.1152/ajprenal.00442.2014.

47. Mei R, Qin W, Zheng Y, Wan Z, Liu L. Role of Adipose Tissue Derived Exosomes in Metabolic Disease. Front Endocrinol (Lausanne). 2022 May 4;13:873865. doi: 10.3389/fendo.2022.873865.

48. Liu Y, Wang C, Wei M, Yang G, Yuan L. Multifaceted Roles of Adipose Tissue-Derived Exosomes in Physiological and Pathological Conditions. Front Physiol. 2021 Apr 20;12:669429. doi: 10.3389/fphys.2021.669429.

49. Martos-Rus C, Katz-Greenberg G, Lin Z, Serrano E, Whitaker-Menezes D, Domingo-Vidal M, et al. Macrophage and adipocyte interaction as a source of inflammation in kidney disease. Sci Rep. 2021 Feb 3;11(1):2974. doi: 10.1038/s41598-021-82685-4.

50. Martinez Cantarin MP, Whitaker-Menezes D, Lin Z, Falkner B. Uremia induces adipose tissue inflammation and muscle mitochondrial dysfunction. Nephrol Dial Transplant. 2017 Jun 1;32(6):943-951. doi: 10.1093/ndt/gfx050.

51. Teplan V, Jr., Vyhnanek F, Gurlich R, Haluzik M, Racek J, Vyhnankova I, et al. Increased proinflammatory cytokine production in adipose tissue of obese patients with chronic kidney disease. Wien Klin Wochenschr. 2010 Aug;122(15-16):466-73. doi: 10.1007/s00508-010-1409-y.